APPENDIX

Supplementary Material to 'Heavy δ^{57}Fe in ocean island basalts:
a non-unique signature of processes and source lithologies in the mantle', Soderman et al.

1 Iron isotope separation methods

1.1 University of Cambridge & Durham University

Iron isotope analyses were carried out on dissolutions of 20 mg of whole-rock powders following established procedures (Williams et al., 2005, 2009). Powders were dissolved in a ∼10:1 mixture of HF:HNO_3 on a hotplate at 120°C for 48 hours, evaporated to dryness and re-dissolved twice in 6 M HCl to remove fluorides. Each dissolution was brought up in 2 ml 6 M HCl, and 500μl loaded onto AG1-X4 anion exchange resin, preconditioned with 6 M HCl. Matrix was eluted using 4 ml 6 M HCl, then iron collected with 7 ml 2 M HCl. The purified Fe solution was dried, refluxed in HNO_3:H_2O_2, and dissolved in 0.1 M HNO_3 for isotopic analysis.

Sample solutions were analysed for Fe isotopes on a ThermoNeptune plus MC-ICP-MS at 6 ppm Fe. Samples were introduced using a quartz cyclonic spray chamber, and instrumental mass bias was corrected for by sample standard bracketing. Sample and standard iron beam intensities (typically 35–45 V ^{56}Fe on a 10^{11} Ω resistor) were matched to within 5%. Mass dependence, reproducibility and accuracy were monitored by analysis of an in-house $FeCl_3$ salt standard and international rock standards (BHVO-2, BIR-1, BCR-2) processed through column chemistry (Table S1), giving values in agreement with previous studies (Williams et al., 2018; Craddock and Dauphas, 2010).

1.2 Isotopia Laboratory, Monash University

Iron isotope analyses were carried out on dissolutions of ∼ 25 mg of whole-rock powders following established procedures (Cheng et al., 2014; Sossi et al., 2015; Ruttor et al., 2020, *subm.*). Powders were dissolved in 2 ml concentrated HF:HNO_3 (ratio 1:2), for a maximum of three days on a hotplate at 120°C and evaporated to dryness once completely dissolved. After evaporation, samples were treated with several drops of concentrated nitric acid to ensure the absence of fluoride bonds. Afterwards, samples were taken up in 9 M HCl and pipetted onto AG-MP-1 anion resin, preconditioned with 9 M HCl. Column chromatographic extraction with 9 M HCl and 5M HCl removed matrix elements as well as semi and transitional metals. The Fe fraction was eluted with 1M HCl. The collected Fe fraction was placed on a hotplate at 90°C. The dried samples were dissolved and taken up in 2% HNO_3.

The Fe isotope analyses were performed on a ThermoFisher^{TM} Scientific Neptune plus MC-ICP-MS in medium-resolution. The samples were introduced via a low flow quartz cyclonic spray chamber and a PFA nebuliser. Each sample was analysed three times from a single dissolution

Table S1: Standard data from all analyses. n = number of repeat analyses.

Standard	δ^{56}Fe (‰)	2 S.D.	δ^{57}Fe (‰)	2 S.D.	n
University of Cambridge					
BIR-1	0.05	0.04	0.07	0.05	8
BCR-2	0.08	0.04	0.13	0.06	12
BHVO-2	0.11	0.04	0.17	0.05	62
$FeCl_3$	−0.73	0.03	−1.08	0.05	61
Durham University					
BIR-1	0.06	0.01	0.08	0.01	2
$FeCl_3$	−0.69	0.03	−1.03	0.05	25
Monash University					
BCR-2	0.10	0.04	0.12	0.04	3

batch in order to ensure precision and accuracy. Isotope ratios for each sample presented here are averaged from these three individual analyses. Each single dissolution batch was mixed with a Ni standard solution to correct for instrumental mass bias effects. To ensure reliability and comparability of our Fe isotope data, the basaltic reference material BCR2 was analysed with the samples. Our analysis are in agreement with previously published analysis. The reproducibility of the method is ± 0.03‰(as a two-standard deviation) in 57Fe/54Fe relative to the IRMM-524a external standard based on repeated analyses of standard reference materials. The reproducibility of each sample was calculated as the standard deviation from 3 repeated analyses. Always the larger error (external vs. sample-averaged error) was used. At the end of the analysis a blank has been analysed and showed values below detection level and is thus negligible.

2 Fractional crystallisation correction

The value of $\Delta^{57}Fe_{ol-melt}$ in the fractional crystallisation correction can be calculated using either experimental or theoretical force constants for the relevant phases

$$\Delta^{57/54}Fe_{ol-melt} = 4284\frac{K_{ol} - K_{melt}}{T^2}, \quad (1)$$

where K_i is the Fe-O force constant in phase i (Sossi and O'Neill, 2017). The force constants for olivine and basaltic melt are 197 and 220 ± 10 N/m respectively (Dauphas et al., 2014; using basaltic glass as a proxy for melt and assuming melt Fe^{3+}/Fe_T = 0.15). Using Eq. 1 gives $\Delta^{57}Fe_{ol-melt} \approx -0.1 \times 10^6/T^2$, producing Δ^{57}Fe corrections of 0.00–0.02‰ for the Samoan dataset, which is less than the internal precision of sample analyses. Considering a more oxidised melt (up to Fe^{3+}/Fe_T = 0.3), and allowing for uncertainties in the olivine force constant, $\Delta^{57}Fe_{ol-melt}$ could increase to $-0.3 \times 10^6/T^2$. Nebel et al. (2019) use $\Delta^{57}Fe_{ol-melt}$ = $-0.4 \times 10^6/T^2$ for Pitcairn samples (corresponding to $\Delta^{57}Fe_{ol-melt}$ of −0.15 – −0.2‰ at magmatic temperatures): using this value gives maximum fractional crystallisation corrections of Δ^{57}Fe = −0.08‰ for the Samoan shield samples, and Δ^{57}Fe = −0.05‰ for the Azores samples.

3 Alteration

As discussed in the main text, there are no correlations between high LOI and low Ba/Rb (Figs. S1, S2) that have previously been used to suggest alteration which may generate δ^{57}Fe heterogeneity in samples (Konter et al., 2016), suggesting alteration has not affected the δ^{57}Fe recorded in the Azores and Samoan samples that are used in this study.

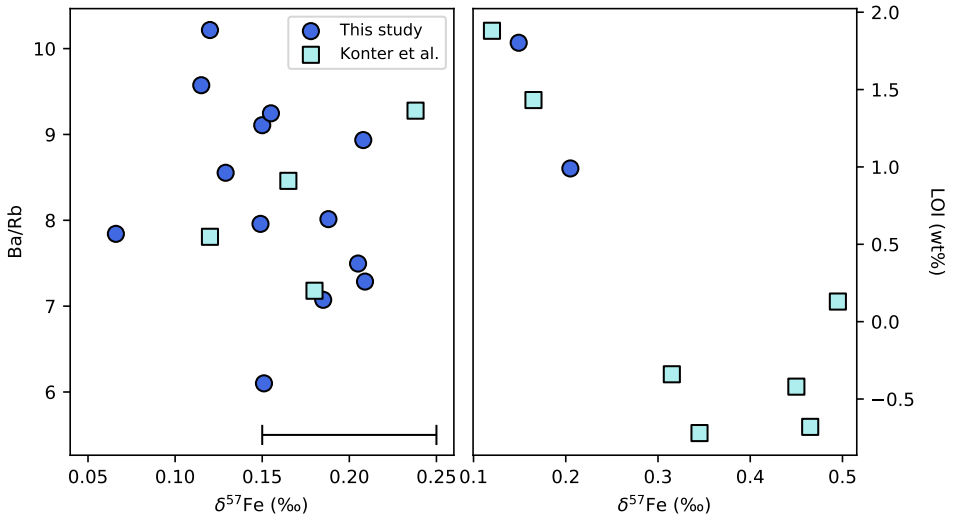

Figure S1: Ba/Rb and LOI for Samoan samples. Errorbar shows long term 2 S.D. of 0.05‰.

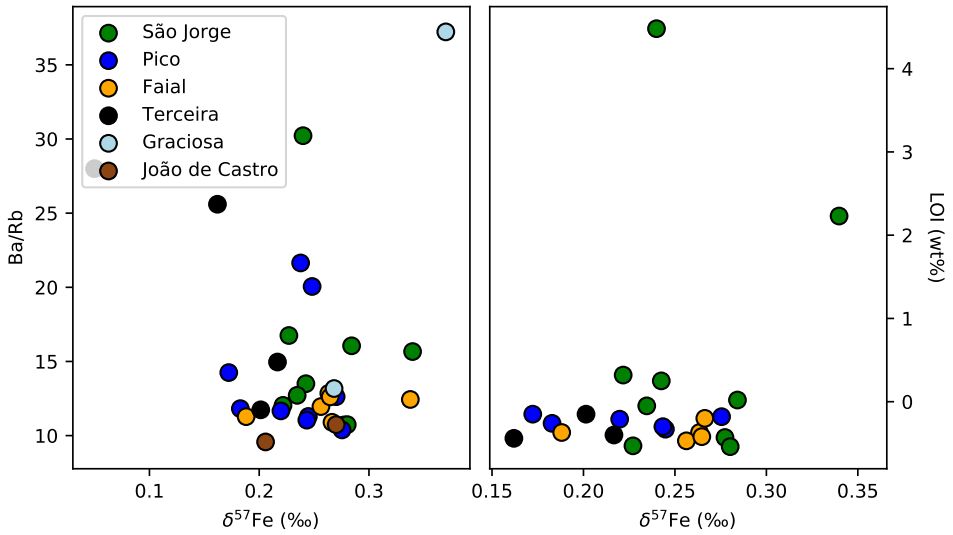

Figure S2: Ba/Rb and LOI for Azores samples.

4 TiO_2 vs MgO

At the onset of magnetite fractionation during crystallisation of a melt, studies have recorded a decrease in whole-rock δ^{57}Fe (e.g., Williams et al., 2018; McCoy-West et al., 2018). This is because magnetite is generally expected to be an isotopically heavy phase (δ^{57}Fe $\leq$ 0.3‰, Shahar et al. 2008; Dauphas et al. 2017), although it may also have a light δ^{57}Fe composition

relative to melt depending on the melt Fe^{3+} content and amount of titanium in the crystallising phase (Schuessler, 2008; Sossi et al., 2012). Consequently, samples that have undergone magnetite fractionation or possible mixing with magnetite-fractionated liquids should be carefully considered in Fe isotope work. All Samoa samples studied plot at higher MgO than magnetite saturation (Fig. S3). However, δ^{57}Fe from two samples from Terceira have slightly low TiO_2 for their MgO, suggesting possible mixing with magnetite-saturated melts (Fig. S4). These samples do not have heavy δ^{57}Fe and therefore we can rule out possible (titano-)magnetite saturation as contributing to the heavy δ^{57}Fe in the Azores. These two samples are not considered in the discussion as their δ^{57}Fe may not represent primary melt composition.

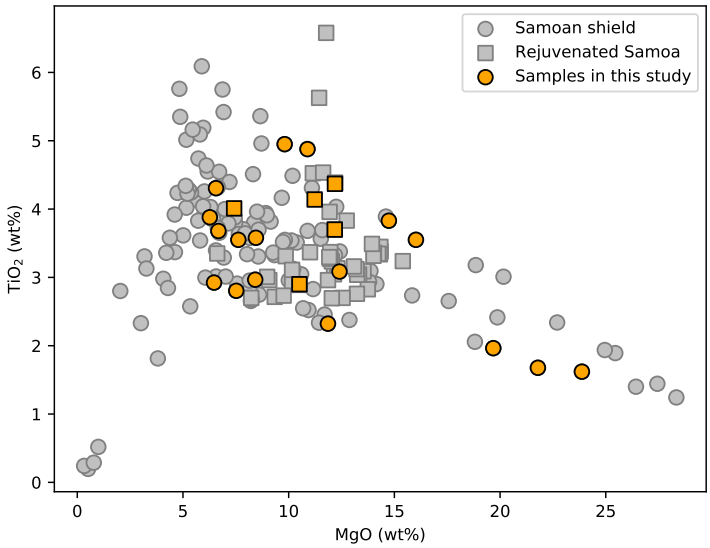

Figure S3: TiO_2 vs MgO for Samoa samples. Grey symbols are published data from Workman et al. (2004); Jackson et al. (2007a); Hart and Jackson (2014); orange symbols highlight samples with δ^{57}Fe measured in this study. There is no difference in TiO_2 between shield and rejuvenated lavas.

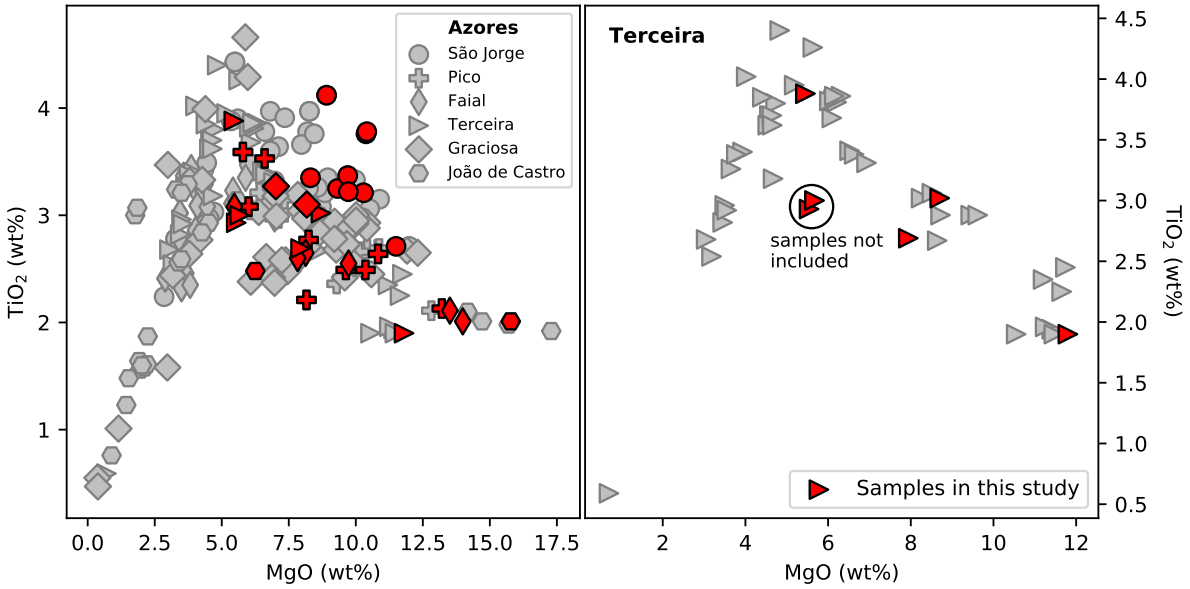

Figure S4: TiO_2 vs MgO for Azores samples. Grey symbols are published data from Turner et al. (1997); Beier et al. (2008); Millet et al. (2009); Beier et al. (2012); Béguelin et al. (2017); Waters et al. (2020); red symbols highlight those samples with δ^{57}Fe measured in this study. The Terceira samples are also shown, highlighting the two low TiO_2 samples not considered in case of mixing with magnetite fractionated melts.

5 Phase equilibria and isotope fractionation model

To explore the partial melting fractionation from pyroxenite and peridotite, we first constructed pseudosections and calculated mineral chemistries for each lithology. The calculations were performed in the KNCFMASTOCr system using THERMOCALC v3.47 (Powell et al., 1998), and the latest version of the thermodynamic dataset (ds-633; Holland et al., 2018) of Holland and Powell (2011).

The compositions of the peridotite and pyroxenite lithologies used in the phase-equilibria calculations are given in Table S2.

Table S2: Lithology compositions, in KNCFMASTOCr system. KLB1 composition from Davis et al. (2009), G2 from Pertermann and Hirschmann (2003), both converted to mole % oxides. Cr added to G2 pyroxenite composition in order to stabilise ThermoCalc model.

	mole % oxide									
	SiO_2	Al_2O_3	CaO	MgO	FeO_t	K_2O	Na_2O	TiO_2	Cr_2O_3	O
KLB1	38.5	1.78	2.82	50.58	5.52	0.01	0.25	0.07	0.11	0.09
G2	52.4	9.72	13.17	12.33	5.64	0.02	3.09	1.55	0.02	0.64

After calculation of the phase boundaries, THERMOCALC was run over a grid of P-T space, from 5–40 kbar and 1100–1930°C. Following the model used in Williams et al. (2020), the equations presented in Sossi and O'Neill (2017) were used to calculate the force constants for Fe-O bonds in each mineral site hosting Fe in olivine, spinel, clinopyroxene, orthopyroxene, ilmenite. The input parameters used are shown in Table S3. For melt, we use the force constants estimated for basaltic melts of varying Fe^3/Fe_T from Dauphas et al. (2014). The force constants are used to calculate fractionation factors between each mineral and melt, and then estimate the deviation of δ^{57}Fe in the magma with respect to the bulk composition of 0.0‰ (i.e., $\Delta^{57}Fe_{melt-bulk}$, the partial melting fractionation).

Table S3: Input parameters for the mineral-melt fractionation model.

Mineral	Fe species	Site	Fe coordination	Bond length (Å)	O coordination	No. sites
spinel	2+	M	6	2.15	4	2
spinel	2+	T	4	2.00	4	1
spinel	3+	M	6	2.03	4	2
spinel	3+	T	4	1.88	4	1
garnet	2+	M1	8	2.29	4	3
garnet	3+	M2	6	2.02	4	2
olivine	2+	M1	6	2.16	4	1
olivine	2+	M2	6	2.18	4	1
orthopyroxene	2+	M1	6	2.14	3.66	1
orthopyroxene	3+	M1	6	2.12	3.66	1
orthopyroxene	2+	M2	6	2.23	3.33	1
clinopyroxene	2+	M1	6	2.14	3.66	1
clinopyroxene	3+	M1	6	2.03	3.66	1
clinopyroxene	2+	M2	6	2.53	3.75	1
ilmenite	2+	A	6	2.14	4	1
ilmenite	3+	B	6	1.98	4	1
ilmenite	3+	A	6	2.14	4	1
ilmenite	2+	B	6	1.98	4	1

6 Influence of core liquids on δ^{57}Fe in OIB

Lesher et al. (2020) have recently proposed that thermodiffusion in core liquids infiltrating into the lowermost mantle could generate a heavy δ^{57}Fe boundary layer just above the CMB. This boundary layer could then be entrained in upwelling mantle plumes and contribute to heavy δ^{57}Fe in OIB melts. This thermodiffusion model predicts that heavy δ^{57}Fe is associated with other core-derived signatures, such as high Fe/Mn (Humayun et al., 2004), or negative μ^{182}W and high ^{3}He/^{4}He (Mundl-Petermeier et al., 2020).

However, no relationship between δ^{57}Fe (corrected for fractional crystallisation) and Fe/Mn (see methods below), μ^{182}W or ^{3}He/^{4}He is seen (Fig. S5). This argues against core-derived liquids being responsible for heavy δ^{57}Fe melts in OIB, although as discussed by Lesher et al. (2020) it is not known how well coupled we might expect Fe and W isotopes to be.

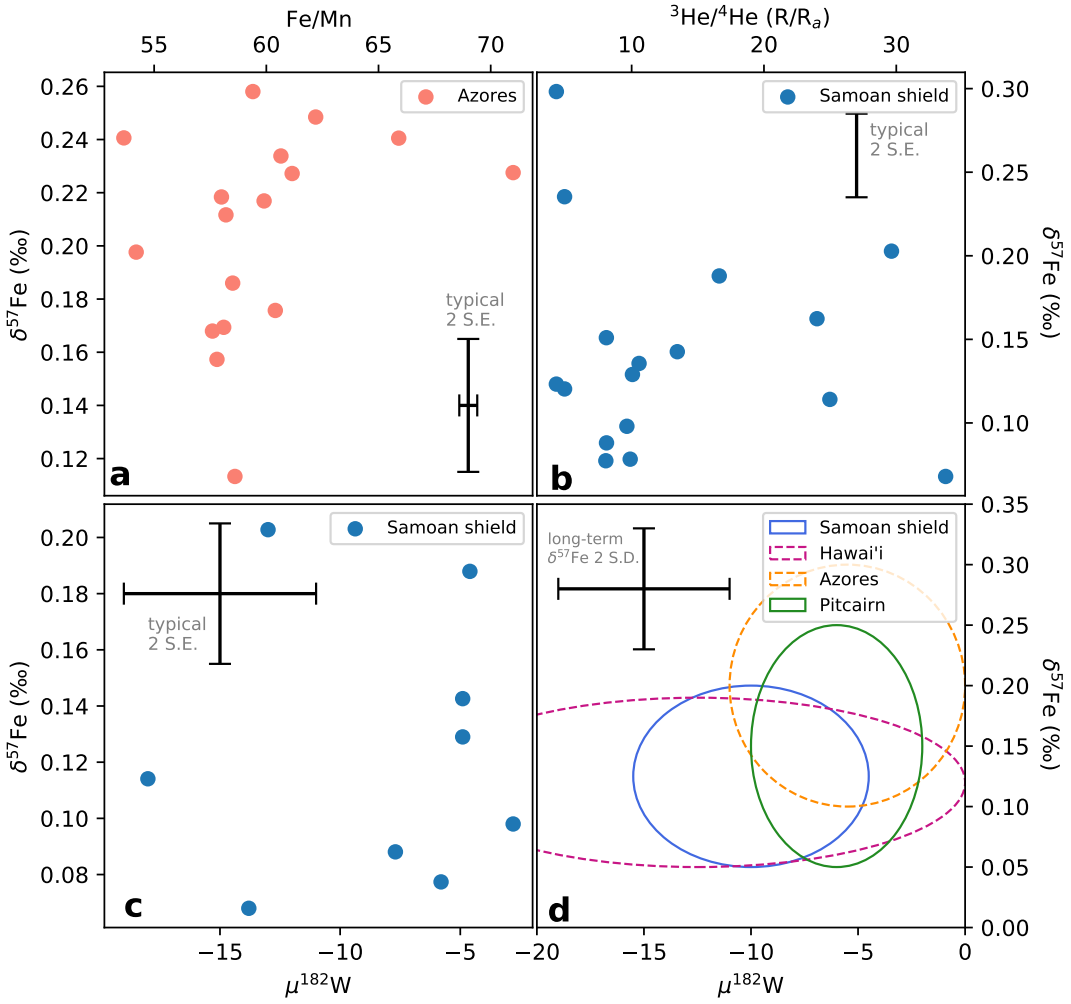

Figure S5: a–c) Available Fe/Mn, μ^{182}W or ^{3}He/^{4}He data for the same samples with δ^{57}Fe measured in this study (corrected for fractional crystallisation). Typical 2 S.E. on μ^{182}W from Mundl-Petermeier et al. (2020), typical 2 S.E. on δ^{57}Fe from average 2 S.E. for repeat analyses of a sample within a sample run. In a), the Fe/Mn data is corrected for fractional crystallisation following procedures described in Section 6.1 below. Error shown on Fe/Mn is a typical error from repeats of the same sample (see Table S4). d) The distribution of δ^{57}Fe and μ^{182}W for 4 plume systems, although these are not necessarily measurements from the same samples. μ^{182}W taken from Mundl-Petermeier et al. (2020), δ^{57}Fe from this study; Konter et al. (2016); Nebel et al. (2019). Long term 2.S.D reproducibility used as δ^{57}Fe errorbar.

6.1 Florida State University: Fe/Mn ratios

Fe/Mn ratios were measured on dissolutions of the same powders used for iron isotope measurements and for which FeO contents had been reported (Turner et al., 1997). An aliquot of about 100 mg of sample powder was weighed into Savillex^{TM} PFA beakers to which 1 ml HNO_3 and 3 ml HF were added. The beakers were sealed and heated at 150°C for about three days, after which the solutions were dried down. The residue was taken up in 6 ml of 6 M HCl, resealed and heated at 150°C overnight to dissolve any residual fluorides. Each PFA vial was heated with 2 ml 12 M HCl to extract any traces of sample remaining, and this solution was combined with the sample stock solution. Ultrapure Seastar^{TM} acids were used in preparing solutions. To avoid loss of volatile $FeCl_3$ none of the HCl-bearing solutions was dried down. The clear solutions were transferred to acid-washed LDPE bottles and diluted to 100 ml with MilliQ^{TM} deionized water to form a matrix with 5% HCl and 0.01% HF. Aliquots for these stock solutions were diluted to form 1% HCl, tr. HF, solutions for ICP-MS analysis.

Precise Fe/Mn ratios were determined on a Thermo Element 1^{TM} at the NHMFL, FSU following procedures described previously (Huang et al., 2007; Qin and Humayun, 2008). Gravimetrically prepared Fe/Mn standards with Fe/Mn ratios from 40–80 were used to prepare a calibration curve. Internal precision was ± 0.2% (1 sigma) and external reproducibility is better than ± 0.5% (1 sigma). Individual basalt rocks vary in their Fe/Mn during fractionation of olivine and clinopyroxene in Azorean magmas with an initial increase in Fe/Mn at high MgO followed by a decrease in Fe/Mn due to clinopyroxene fractionation producing a convex-upward curve in a plot of Fe/Mn vs. MgO. Each island produced distinct curves for Fe/Mn vs. MgO but, because of the small number of samples from each island, a single quadratic fit was used for Pico, Faial and Terceira and applied to samples from São Miguel and São Jorge that had significantly higher scatter around the curve. The Fe/Mn of each sample was corrected to 8 wt% MgO using the quadratic interpolation, and an average reported for each island (Table S4). Since prior work has shown that the errors in published Fe/Mn data is due to the errors in MnO, following Huang et al. (2007) precise MnO abundances were calculated from the measured Fe/Mn ratios and the reported FeO_T abundances (Turner et al., 1997).

The Fe/Mn ratios of the Azores define two groups: volcanics from the islands of Pico, Faial and Terceira are similar to those from Iceland (Humayun et al., 2004; Qin and Humayun, 2008), while volcanics from São Jorge and São Miguel exhibit variations in Fe/Mn that range (60–68) between Icelandic and Hawaiian lavas (Humayun et al., 2004; Huang et al., 2007). Since Fe isotope data from São Miguel samples are not presented in this manuscript, there is little reason to expect a strong core-mantle exchange effect on the Fe isotope dataset presented here from the Fe/Mn, with the exception of some São Jorge samples.

7 Carbonatite in the Azores source

Carbonated peridotite melts can be identified by their fractionation of trace and major element ratios, including Nb/La, Ti/Sm and K/La (Cottrell and Kelley, 2013; Beier et al., 2013) relative to anhydrous peridotite melts. The Azores volcano of Santa Maria has been proposed to require at least 20% of a 1% carbonated peridotite melt in its source based on Ti/Sm and K/La (Beier et al., 2013), however the other volcanoes that are sampled in this study do not show evidence for a carbonated peridotite component in the source (Fig. S6). Consistent with this, the measured δ^{57}Fe show no correlations with proposed tracers of carbonatite melt from Cottrell and Kelley

(2013); Beier et al. (2013); Fig. S7.

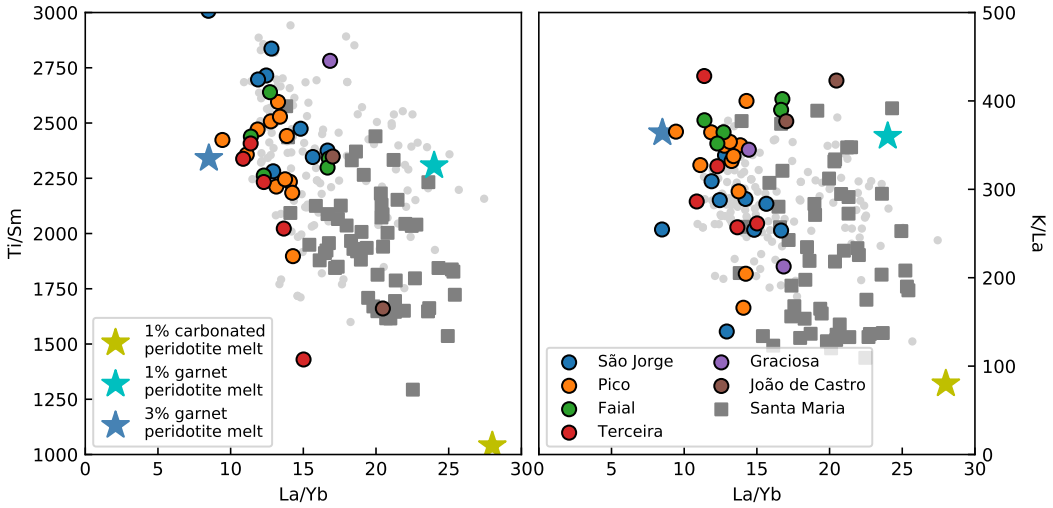

Figure S6: Ti/Sm and K/La vs La/Yb for Azores samples measured in this study (coloured circles, filtered for those > 5.5 wt% MgO) compared to Santa Maria (Beier et al., 2013), an Azores volcano thought to sample a carbonated peridotite source. Compilation of Azores volcanoes, published by Béguelin et al. (2017), shown in small pale grey circles for reference. The coloured stars show modelled melts from carbonated and garnet peridotite sources calculated in Beier et al. (2013), highlighting the low Ti/Sm and K/La expected from carbonated peridotite melts.

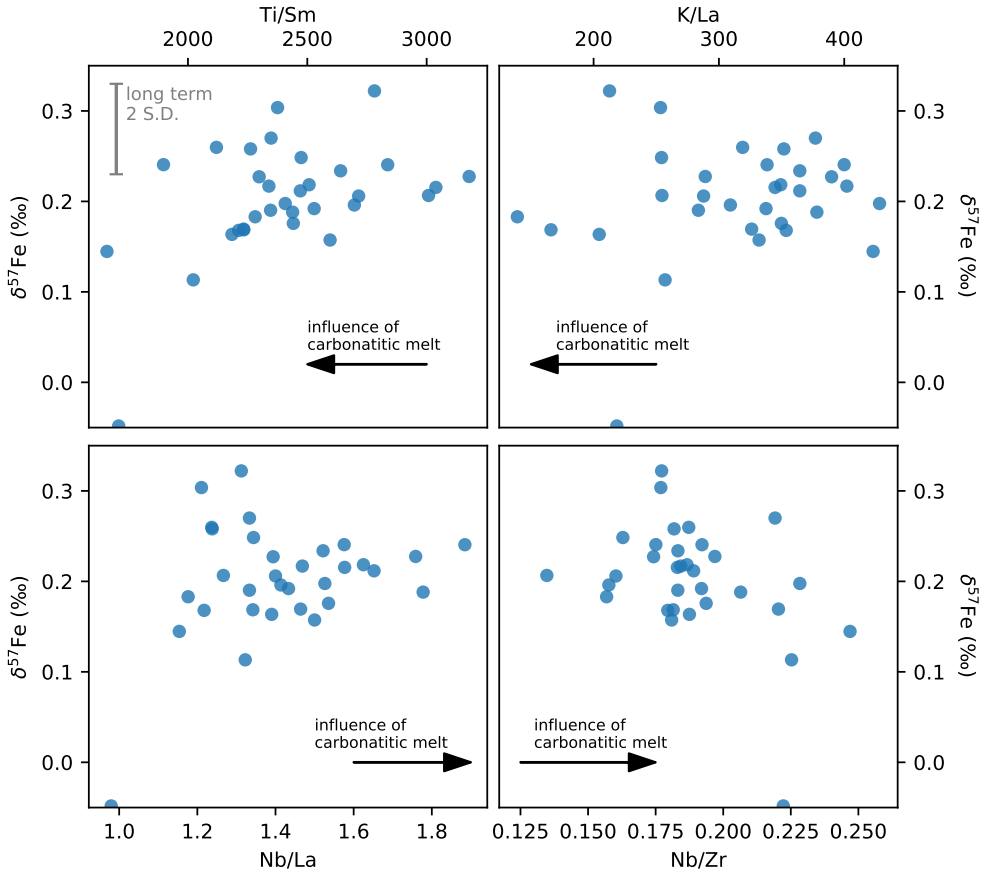

Figure S7: Measured δ^{57}Fe in Azores lavas (corrected for fractional crystallisation) show no relationship to tracers of carbonatite melts in their source region. Major and trace element data from Turner et al. (1997); Beier et al. (2008); Millet et al. (2009); Beier et al. (2012); Béguelin et al. (2017); Waters et al. (2020).

Table S4: Fe/Mn data for Azorean samples (samples in italics not measured for Fe isotopes). See references in Table 1 in main manuscript for major element sources. Averages include samples not measured for Fe isotopes. rep = replicate.

Sample	FeO_T (wt%)	MnO (calc)	MgO (wt%)	Fe/Mn measured	Fe/Mn, corr. 8 wt% MgO
Terceira					
T2	10.52	0.203	5.54	52.0	57.8
T2 rep	10.52	0.206	5.54	51.3	57.1
T6	11.01	0.183	8.70	60.4	59.2
T6 rep	11.01	0.187	8.70	59.2	58.0
T18	10.46	0.179	7.94	58.7	58.8
T18 rep	10.46	0.183	7.94	57.3	57.4
WAT3	9.04	0.155	11.80	58.4	54.2
Average	10.43	0.185		56.8	**57.5**
st.dev.	6%	9%		6%	3%
Pico					
P4	9.92	0.164	10.36	60.8	57.4
P4 rep	9.92	0.162	10.36	61.6	58.2
P5	9.79	0.162	9.63	60.8	58.2
P25	9.98	0.165	8.24	60.9	60.4
P26	10.27	0.167	10.83	61.8	58.0
P29	9.30	0.175	8.16	53.4	53.1
P29 rep	9.30	0.171	8.16	54.5	54.2
WAP9	10.04	0.162	13.21	62.0	57.6
WAP10	*8.04*	*0.138*	*17.63*	*58.6*	*58.8*
WAP25	*10.48*	*0.170*	*14.34*	*61.9*	*57.9*
Average	9.70	0.163		59.6	**57.4**
st.dev.	7%	6%		5%	4%
Faial					
F/CA-6	9.65	0.154	9.73	62.9	60.2
F/CA-6 rep	9.65	0.152	9.73	63.8	61.1
F/CA-24	9.94	0.160	15.05	62.0	58.5
F/CP-18	9.30	0.155	7.83	60.2	60.6
F/CP-18 rep	9.30	0.152	7.83	61.3	61.7
F/FG-28	9.74	0.162	8.13	60.2	59.9
WAF1a	9.98	0.157	13.51	63.8	59.4
Average	9.65	0.156		62.0	**60.2**
st. dev.	3%	3%		2%	2%
São Jorge					
WASJ18	10.48	0.162	9.72	64.9	62.2
SJ30	11.32	0.166	9.70	68.5	65.9
SJ31b	12.38	0.171	8.91	72.6	71.0
SJ48	*11.04*	*0.180*	*7.52*	*61.7*	*62.7*
SJ76	*11.27*	*0.191*	*9.10*	*59.1*	*57.3*
SJ77	*12.73*	*0.177*	*8.85*	*72.1*	*70.7*
SJ84	*11.34*	*0.177*	*8.26*	*64.2*	*63.7*
SJ101	*10.76*	*0.171*	*8.90*	*63.1*	*61.5*
Average	11.42	0.174		65.8	**64.4**
st. dev.	7%	5%		7%	7%
São Miguel					
S1	*12.38*	*0.187*	*7.76*	*66.6*	*67.0*
S3	*11.59*	*0.181*	*8.34*	*64.3*	*63.7*
S7	*12.16*	*0.184*	*6.69*	*66.3*	*69.1*
S7 rep	*12.16*	*0.182*	*6.69*	*66.9*	*69.7*
S10	*11.76*	*0.175*	*8.33*	*67.6*	*67.0*
S10 rep	*11.76*	*0.173*	*8.33*	*68.3*	*67.7*
SP2	*12.23*	*0.184*	*7.93*	*66.5*	*66.7*
SP8	*10.70*	*0.169*	*9.10*	*63.6*	*61.7*
WASM1	*11.52*	*0.168*	*11.16*	*68.7*	*64.8*
WASM5	*12.10*	*0.172*	*11.26*	*70.7*	*66.7*
WASM24	*11.13*	*0.173*	*10.55*	*64.5*	*60.9*
WASM33	*11.44*	*0.173*	*12.28*	*66.5*	*62.1*
Average	*11.74*	*0.177*		*66.7*	*65.6*
st. dev.	*4%*	*4%*		*3%*	*4%*

References

Béguelin, P., Bizimis, M., Beier, C. and Turner, S. (2017), 'Rift–plume interaction reveals multiple generations of recycled oceanic crust in Azores lavas', *Geochimica et Cosmochimica Acta* **218**, 132–152.

Beier, C., Haase, K. M., Abouchami, W., Krienitz, M.-S. and Hauff, F. (2008), 'Magma genesis by rifting of oceanic lithosphere above anomalous mantle: Terceira Rift, Azores', *Geochemistry, Geophysics, Geosystems* **9**(12).

Beier, C., Haase, K. M. and Turner, S. P. (2012), 'Conditions of melting beneath the Azores', *Lithos* **144**, 1–11.

Beier, C., Mata, J., Stöckhert, F., Mattielli, N., Brandl, P. A., Madureira, P., Genske, F. S., Martins, S., Madeira, J. and Haase, K. M. (2013), 'Geochemical evidence for melting of carbonated peridotite on Santa Maria Island, Azores', *Contributions to Mineralogy and Petrology* **165**(5), 823–841.

Cheng, T., Nebel, O., Sossi, P. A. and Chen, F. (2014), 'Refined separation of combined Fe–Hf from rock matrices for isotope analyses using AG-MP-1M and Ln-Spec chromatographic extraction resins', *MethodsX* **1**, 144–150.

Cottrell, E. and Kelley, K. A. (2013), 'Redox heterogeneity in mid-ocean ridge basalts as a function of mantle source', *Science* **340**(6138), 1314–1317.

Craddock, P. R. and Dauphas, N. (2010), 'Iron Isotopic Compositions of Geological Reference Materials and Chondrites', *Geostandards and Geoanalytical Research* **35**(1), 101–123.

Dauphas, N., John, S. G. and Rouxel, O. (2017), 'Iron isotope systematics', *Reviews in Mineralogy and Geochemistry* **82**(1), 415–510.

Dauphas, N., Roskosz, M., Alp, E., Neuville, D., Hu, M., Sio, C., Tissot, F., Zhao, J., Tissandier, L., Médard, E. et al. (2014), 'Magma redox and structural controls on iron isotope variations in Earth's mantle and crust', *Earth and Planetary Science Letters* **398**, 127–140.

Davis, F. A., Tangeman, J. A., Tenner, T. J. and Hirschmann, M. M. (2009), 'The composition of KLB-1 peridotite', *American Mineralogist* **94**(1), 176–180.

Hart, S. R. and Jackson, M. G. (2014), 'Ta'u and Ofu/Olosega volcanoes: The "Twin Sisters" of Samoa, their P, T, X melting regime, and global implications', *Geochemistry, Geophysics, Geosystems* **15**(6), 2301–2318.

Holland, T. J. B., Green, E. C. R. and Powell, R. (2018), 'Melting of Peridotites through to Granites: A Simple Thermodynamic Model in the System KNCFMASHTOCr', *Journal of Petrology* **59**(5), 881–900.

Holland, T. and Powell, R. (2011), 'An improved and extended internally consistent thermodynamic dataset for phases of petrological interest, involving a new equation of state for solids', *Journal of Metamorphic Geology* **29**(3), 333–383.

Huang, S., Humayun, M. and Frey, F. A. (2007), 'Iron/manganese ratio and manganese content in shield lavas from Ko'olau Volcano, Hawai'i', *Geochimica et Cosmochimica Acta* **71**(18), 4557–4569.

Humayun, M., Qin, L. and Norman, M. D. (2004), 'Geochemical evidence for excess iron in the mantle beneath hawaii', *Science* **306**(5693), 91–94.

Jackson, M. G., Kurz, M. D., Hart, S. R. and Workman, R. K. (2007a), 'New Samoan lavas from Ofu Island reveal a hemispherically heterogeneous high $^{3}He/^{4}He$ mantle', *Earth and Planetary Science Letters* **264**(3-4), 360–374.

Konter, J. G., Pietruszka, A. J., Hanan, B. B., Finlayson, V. A., Craddock, P. R., Jackson, M. G. and Dauphas, N. (2016), 'Unusual δ^{56} Fe values in Samoan rejuvenated lavas generated in the mantle', *Earth and Planetary Science Letters* **450**, 221–232.

Lesher, C. E., Dannberg, J., Barfod, G. H., Bennett, N. R., Glessner, J. J., Lacks, D. J. and Brenan, J. M. (2020), 'Iron isotope fractionation at the core–mantle boundary by thermodiffusion', *Nature Geoscience* pp. 1–5.

McCoy-West, A. J., Fitton, J. G., Pons, M.-L., Inglis, E. C. and Williams, H. M. (2018), 'The Fe and Zn isotope composition of deep mantle source regions: Insights from Baffin Island picrites', *Geochimica et Cosmochimica Acta* **238**, 542–562.

Millet, M.-A., Doucelance, R., Baker, J. A. and Schiano, P. (2009), 'Reconsidering the origins of isotopic variations in Ocean Island Basalts: insights from fine-scale study of São Jorge Island, Azores archipelago', *Chemical Geology* **265**(3-4), 289–302.

Mundl-Petermeier, A., Walker, R., Fischer, R., Lekic, V., Jackson, M. and Kurz, M. (2020), 'Anomalous 182W in high 3He/4He ocean island basalts: Fingerprints of Earth's core?', *Geochimica et Cosmochimica Acta* **271**, 194–211.

Nebel, O., Sossi, P. A., Bénard, A., Arculus, R. J., Yaxley, G. M., Woodhead, J. D., Davies, D. R. and Ruttor, S. (2019), 'Reconciling petrological and isotopic mixing mechanisms in the Pitcairn mantle plume using stable Fe isotopes', *Earth and Planetary Science Letters* **521**, 60–67.

Pertermann, M. and Hirschmann, M. M. (2003), 'Partial melting experiments on a MORB-like pyroxenite between 2 and 3 GPa: Constraints on the presence of pyroxenite in basalt source regions from solidus location and melting rate', *Journal of Geophysical Research: Solid Earth* **108**(B2).

Powell, R., Holland, T. and Worley, B. (1998), 'Calculating phase diagrams involving solid solutions via non-linear equations, with examples using THERMOCALC', *Journal of Metamorphic Geology* **16**(4), 577–588.

Qin, L. and Humayun, M. (2008), 'The Fe/Mn ratio in MORB and OIB determined by ICP-MS', *Geochimica et Cosmochimica Acta* **72**(6), 1660–1677.

Ruttor, S., Nebel, O., Williams, H. M., Beier, C., Richter, M., Nebel-Jacobsen, Y., Romer, R. and Turner, S. (2020), 'Stable iron isotopes as a tracer for mantle plume components at São Miguel, Azores: implications for the FOZO plume matrix', *Earth and Planetary Science Letters* .

Schuessler, J. A. (2008), Controls on stable iron isotope variations in magmetic systems, PhD thesis, Hannover.

Shahar, A., Young, E. D. and Manning, C. E. (2008), 'Equilibrium high-temperature Fe isotope fractionation between fayalite and magnetite: an experimental calibration', *Earth and Planetary Science Letters* **268**(3-4), 330–338.

Sossi, P. A., Foden, J. D. and Halverson, G. P. (2012), 'Redox-controlled iron isotope fractionation during magmatic differentiation: an example from the Red Hill intrusion, S. Tasmania', *Contributions to Mineralogy and Petrology* **164**(5), 757–772.

Sossi, P. A., Halverson, G. P., Nebel, O. and Eggins, S. M. (2015), 'Combined separation of Cu, Fe and Zn from rock matrices and improved analytical protocols for stable isotope determination', *Geostandards and Geoanalytical Research* **39**(2), 129–149.

Sossi, P. A. and O'Neill, H. S. C. (2017), 'The effect of bonding environment on iron isotope fractionation between minerals at high temperature', *Geochimica et Cosmochimica Acta* **196**, 121–143.

Turner, S., Hawkesworth, C., Rogers, N. and King, P. (1997), 'U-Th isotope disequilibria and ocean island basalt generation in the Azores', *Chemical Geology* **139**(1-4), 145–164.

Waters, C. L., Day, J. M., Watanabe, S., Sayit, K., Zanon, V., Olson, K. M., Hanan, B. B. and Widom, E. (2020), 'Sulfide mantle source heterogeneity recorded in basaltic lavas from the azores', *Geochimica et Cosmochimica Acta* **268**, 422–445.

Williams, H. M., Nielsen, S. G., Renac, C., Griffin, W. L., O'Reilly, S. Y., McCammon, C. A., Pearson, N., Viljoen, F., Alt, J. C. and Halliday, A. N. (2009), 'Fractionation of oxygen and iron isotopes by partial melting processes: Implications for the interpretation of stable isotope signatures in mafic rocks', *Earth and Planetary Science Letters* **283**(1-4), 156–166.

Williams, H. M., Peslier, A. H., McCammon, C., Halliday, A. N., Levasseur, S., Teutsch, N. and Burg, J.-P. (2005), 'Systematic iron isotope variations in mantle rocks and minerals: the effects of partial melting and oxygen fugacity', *Earth and Planetary Science Letters* **235**(1-2), 435–452.

Williams, H., Matthews, S., Rizo, H. and Shorttle, O. (2020), 'Iron isotopes trace primordial magma ocean cumulates melting in the Earth's upper mantle', *Science Advances (subm.)* .

Williams, H., Prytulak, J., Woodhead, J., Kelley, K., Brounce, M. and Plank, T. (2018), 'Interplay of crystal fractionation, sulfide saturation and oxygen fugacity on the iron isotope composition of arc lavas: An example from the Marianas', *Geochimica et Cosmochimica Acta* **226**, 224 – 243.

Workman, R. K., Hart, S. R., Jackson, M., Regelous, M., Farley, K. A., Blusztajn, J., Kurz, M. and Staudigel, H. (2004), 'Recycled metasomatized lithosphere as the origin of the Enriched Mantle II (EM2) end-member: Evidence from the Samoan volcanic chain', *Geochemistry, Geophysics, Geosystems* **5**(4), n/a–n/a.